

UC Irvine

UC Irvine Previously Published Works

Title

Mobilization of aged and biolabile soil carbon by tropical deforestation

Permalink

<https://escholarship.org/uc/item/45n6x8tn>

Journal

Nature Geoscience, 12(7)

ISSN

1752-0894

Authors

Drake, Travis W
Van Oost, Kristof
Barthel, Matti
[et al.](#)

Publication Date

2019-07-01

DOI

10.1038/s41561-019-0384-9

Copyright Information

This work is made available under the terms of a Creative Commons Attribution License, available at <https://creativecommons.org/licenses/by/4.0/>

Peer reviewed

Published in final edited form as:

Nat Geosci. 2019 June 10; 12(7): 541–546. doi:10.1038/s41561-019-0384-9.

Mobilization of aged and biolabile soil carbon by tropical deforestation

Travis W. Drake^{1,2,*†}, Kristof Van Oost³, Matti Barthel⁴, Marijn Bateurs^{5,6}, Alison M. Hoyt^{7,8}, David C. Podgorski^{1,2,‡}, Johan Six⁴, Pascal Boeckx⁵, Susan E. Trumbore^{7,9}, Landry Cizungu Ntaboba¹⁰, Robert G. M. Spencer^{1,2}

¹Department of Earth, Ocean, and Atmospheric Science, Florida State University, Tallahassee, FL, USA

²National High Magnetic Field Laboratory Geochemistry Group, Tallahassee, FL, USA

³Earth and Life Institute, Université Catholique de Louvain, Louvain-la-Neuve, Belgium

⁴Department of Environmental Systems Science, ETH Zurich, Switzerland

⁵Isotope Bioscience Laboratory, Department of Green Chemistry and Technology, Ghent University, 9000 Gent, Belgium

⁶Computational & Applied Vegetation Ecology Lab, Department of Environment, Ghent University, 9000 Gent, Belgium

⁷Max Planck Institute for Biogeochemistry, 07745 Jena, Germany

⁸Lawrence Berkeley National Laboratory, Berkeley, CA, 94720 USA

⁹Earth System Science, University of California, Irvine, CA, USA

¹⁰Faculty of Agronomy, Université Catholique de Bukavu, BP 285 Bukavu, Democratic Republic of Congo

Introductory Paragraph

In the mostly pristine Congo Basin, agricultural land-use change has intensified in recent years. One potential and understudied consequence of this deforestation and conversion to agriculture is the mobilization and loss of organic matter from soils to rivers as dissolved organic matter. Here, we quantify and characterize dissolved organic matter sampled from 19 catchments of varying deforestation extent near Lake Kivu over a two-week period during the wet season. Dissolved organic carbon from deforested, agriculturally-dominated catchments was older (¹⁴C age: ~1.5kyr) and more biolabile than from pristine forest catchments. Ultrahigh-resolution mass spectrometry revealed that this aged organic matter from deforested catchments was energy-rich and chemodiverse, with higher proportions of nitrogen- and sulfur-containing formulae. Given the

Users may view, print, copy, and download text and data-mine the content in such documents, for the purposes of academic research, subject always to the full Conditions of use:http://www.nature.com/authors/editorial_policies/license.html#terms

*Corresponding author. tel.: +1-503-806-0727; Requests for materials should be addressed to T.W.D. (draketw@gmail.com).

†Now at: Department of Environmental Systems Science, ETH Zurich, Switzerland

‡Now at: Pontchartrain Institute for Environmental Sciences, Department of Chemistry, University of New Orleans, New Orleans, LA 70148, USA

Author Contributions

T.W.D., R.G.M.S., J.S., and K.V.O. conceived of the study. T.W.D., M.B., and M.B. carried out the fieldwork and sample collection. T.W.D., M.B., M.B., A.M.H., and D.C.P. performed sample analyses. T.W.D., K.V.O., and M.B. performed geospatial analyses. L.C.N. provided logistical support in DR Congo. T.W.D. wrote the manuscript with significant contributions from M.B., A.M.H., J.S., P.B., S.E.T. and R.G.M.S.

Data Availability Statement

The authors declare that all data supporting the findings of this study other than non-categorized FT-ICR MS data are available within the paper and its supplementary information files. Non-categorized FT-ICR MS formulae data are available from the corresponding author upon request.

molecular composition and biolability, we suggest that organic matter from deforested landscapes is preferentially respired upon disturbance, resulting in elevated in-stream concentrations of carbon dioxide. We estimate that while deforestation reduces the overall flux of dissolved organic carbon by ~56%, it does not significantly change the yield of biolabile dissolved organic carbon. Ultimately, the exposure of deeper soil horizons through deforestation and agricultural expansion releases old, previously stable, and biolabile soil organic carbon into the modern carbon cycle via the aquatic pathway.

Keywords

dissolved organic carbon; soil organic carbon; deforestation; agriculture; Congo

Introduction

Tropical soils are major reservoirs of soil organic carbon (SOC) and are estimated to contain approximately one-third of the global first-meter SOC stock (~1325 Pg)¹. The stability of these vast tropical SOC stocks is threatened by increasing anthropogenic disturbance in the form of deforestation and associated land-use change. A recent global meta-analysis found that the conversion of tropical primary forest to croplands resulted in an average relative SOC loss of 25%². Given the relevance of these stocks to the global carbon (C) cycle, there is a growing need for fundamental and mechanistic research into how anthropogenic pressures may alter the tropical C cycle.

It is well established that deforestation and land-use change release carbon dioxide (CO₂) via the *in-situ* respiration of SOC in disturbed soils²⁻⁵. A relatively understudied effect of soil disturbance, however, is the leaching and mobilization of SOC as dissolved organic carbon (DOC)⁶. In northern ecosystems, forest loss and soil disturbance has generally been found to increase DOC losses to streams⁷⁻⁹, although decreases have also been reported^{10,11}. The effect of deforestation on DOC mobilization in tropical ecosystems is not well documented, but recent work in SE Asia has shown increases following forest loss, secondary regrowth, and increased freshwater fluxes^{12,13}. In addition to changes in DOC concentration and fluxes, the export of aged DOC has been documented in disturbed soils and is shown to be positively correlated with human disturbance globally, suggesting that DOC is an important indicator of SOC stability^{12,14,15}. Historically, aged DOC sourced from terrestrial ecosystems is assumed to be chemically stable and resistant to biodegradation^{16,17}. Recent studies on aged DOC in Arctic aquatic ecosystems and elsewhere, however, suggest that it can be highly biolabile and rapidly oxidized by microbes upon release to surface waters, depending on the physico-chemical conditions under which it was developed and preserved (i.e. in complexes with minerals, permafrost, anoxia, reducing conditions, etc.)¹⁸⁻²⁰. Little is known about the relationship between DOC biolability and age within tropical ecosystems. Bridging this knowledge gap is important given that the 'lateral' aquatic loss of aged DOC reintroduces aged C into the modern C cycle and is thus analogous to the combustion of fossil fuels, provided the mobilized C is microbially or photo-oxidized to CO₂.

Central Africa's relatively understudied Congo Basin (~3.7 million km²) represents an ideal tropical forest ecosystem to investigate these processes. The Congo Basin is estimated to contain 20 Pg of SOC in its top meter of soil²¹, not including the more than 30 Pg recently mapped and quantified in the inundated swamp forests of the *Cuvette Centrale*²². Currently, the extensive SOC reservoir in the Congo Basin is mostly undisturbed, as the interior lowland forests that protect the soils have remained relatively free from intensive deforestation^{23,24}. Deforestation near the Basin's eastern and western borders, however, has accelerated due to rapid population growth concurrent with agricultural expansion and charcoal production. For example, the Kivu region of eastern Democratic Republic of Congo (DRC) is estimated to have lost more than 2,400 km² of primary forest from 2000 to 2010, ~2.7% of the region's forest cover²⁵.

To assess the impact of deforestation and subsequent conversion to agricultural lands on lateral C losses from tropical soils of the Congo Basin, we measured the concentration, age, and biolability of DOC, in addition to the composition of dissolved organic matter (DOM) exported by 19 catchments of varying deforestation extent near Lake Kivu, DRC. Prior to human settlement and agricultural proliferation in the region, South Kivu was covered by dense tropical forest²⁶. Today, the remaining pristine forests in the region are protected within the borders of Kahuzi-Biéga National Park. Our 19 study catchments span 0.7° latitude, range in area from 0.25 to 85.2 km², and vary by extent of deforestation from 0.0 to 100.0% (Fig. 1).

Mobilization of Aged Sub-Soil C with Land-use Conversion

Our isotopic results point to land-use as a primary control of DOC source and age. The extent of deforestation within a catchment, predominantly a function of agricultural land-use, was negatively related to the bulk radiocarbon age of DOC (Fig. 2a, Table S1). The DOC from completely deforested catchments had a bulk ¹⁴C value of $-179 \pm 16\%$, representing a radiocarbon age of ~1,500 yr BP. These deforested tropical Congo ¹⁴C-DOC values were slightly more enriched but similar to those measured from other disturbed temperate and Amazonian catchments (-230% for urban or agricultural watersheds)¹⁴. In contrast, the pristine catchments draining areas of Kahuzi-Biéga National Park with 100% forest cover displayed a bulk ¹⁴C-DOC value of $+19.0 \pm 17.9\%$, indicating the export of modern DOC.

Deforestation extent was positively correlated with $\delta^{13}\text{C}$ -DOC enrichment (Fig. 2b, Table S1), with fully deforested and forested values of -22.3 ± 0.4 and $-27.4 \pm 0.5\%$, respectively. A coupled isotopic ¹⁴C and $\delta^{13}\text{C}$ -DOC plot shows how deforestation results in both older and more $\delta^{13}\text{C}$ enriched values (colored points, Fig 2c). Soil isotopic signatures to 75cm from the pristine forest of Kahuzi-Biéga National Park revealed a very similar ¹⁴C vs. $\delta^{13}\text{C}$ -SOC gradient with depth as DOC with deforestation (black dotted line, Fig 2c, Table S2). Organic carbon from litter and O-horizons was modern and relatively depleted in $\delta^{13}\text{C}$ (-28.5%), whereas deeper horizons became older and more enriched in $\delta^{13}\text{C}$ (Fig 2c, Table S2). $\delta^{13}\text{C}$ -SOC enrichment profiles like the one observed in Kahuzi-Biéga National Park are generally attributed to higher contributions of microbially-derived and processed C with depth²⁷ and the Suess effect²⁸. Together, these coupled DOC and SOC isotopic values

suggest that deforested catchments export aged C from deeper soil horizons while forest-dominated catchments export modern terrestrial C leached from near the soil surface.

Changing DOM Composition with Land-use Conversion

In addition to DOC age and source, the molecular composition of DOM was strongly controlled by the extent of deforestation in a catchment. Using ultrahigh-resolution mass spectrometry (FT-ICR MS, see methods) of solid-phase extractable DOM, we detected 17,560 distinct molecular formulae across all catchments, with an average of 10,493 formulae present in each sample (Table S3). The average mass and aromaticity index, a measure of molecular stability with regard to biological degradation²⁹, of DOM were found to be negatively correlated with deforestation extent (Fig S1a and b, respectively). In other words, DOM mobilized from deforested catchments was on average smaller and less aromatic in character than DOM exported from forested catchments, suggesting that it is vulnerable to microbial degradation. The chemodiversity of DOM, defined as the presence and proportion of other elements besides C and H, such as oxygen (O), nitrogen (N), and sulfur (S), is another important indicator of DOM source and quality³⁰. Past studies have shown that anthropogenically impacted river catchments export DOM with greater relative abundances of N- and S-containing formula^{30,31}. On average, DOM from deforested catchments in this study exhibited higher fractions of N- and S-containing formulae (CHON and CHOS, respectively) relative to pristine catchments (Fig S2, Table S3).

Furthermore, the fraction of a sample's total relative abundance (signal magnitude) comprised by formula classified as peptide-like, polyphenolic, unsaturated phenolic low-O/C, sugar-like, and condensed aromatic (see supplemental methods), were all found to be significantly correlated with deforestation extent. The fraction of total relative abundance from peptide-like and unsaturated phenolic low-O/C molecules increased with deforestation extent (Fig S1c and d), while polyphenols, condensed aromatics, and sugar-like decreased (Fig S1e, f, g, Table S3). The fraction of total relative abundance from aliphatics and unsaturated high-O/C phenolics did not significantly correlate with deforestation extent (Fig. S1h and i, Table S3). These compound class results show that DOM sourced from deforested soils is highly reduced and more likely to contain N compared to DOM sourced from pristine, forested catchments.

To delve beyond the broad compound classes and assess how the relative abundances of individual molecular formula correlated with deforestation extent and other environmental variables, we performed Spearman's rank correlations for each formula present in more than 50% of all samples (to include formulae sourced uniquely from forested or deforested end-members). FT-ICR MS detected 10,115 formulae present in at least half of all samples, 5,270 (52.1%) of which had relative abundances that were significantly correlated with deforestation extent (average absolute-value Spearman's rank correlation coefficient, $\rho_s = 0.64$; $p < 0.05$). Formulae with similar ρ_s values and signs were found to be grouped into two distinct assemblages in van Krevelen space (Fig. 3a). Formulae with relative intensities that were positively correlated with deforestation extent ($\rho_s > 0$) generally had high H/C and moderately-low O/C ratios, whereas negatively correlated formulae ($\rho_s < 0$) displayed the opposite trend with the exception of one small cluster of high H/C (~1.25) and low O/C

(~0.3) formulae commonly ascribed to lipid-like compounds³². Nearly identical groups of formulae were found to be correlated with $\delta^{13}\text{C}$ -DOC (Fig. 3b) and biolabile DOC (BDOC, Fig. 3c). When formulae relative abundances were correlated with forest extent, ^{14}C -DOC, and DOC concentration, the same two assemblages emerged with inverse coefficient signs (Fig 3d, e, and f).

The two compositional assemblages revealed by FT-ICR MS correspond well to modern forest vegetation and aged SOC as end-member sources for exported DOM. Vascular plant derived DOM is generally low H/C, high O/C, and aromatic in nature^{33–35}, similar to the assemblage of formulae positively correlated with forest extent (Fig. 3d). Aged SOC, however, displays a composition similar to microbial biomass, with high H/C ratios, high N content from proteins, and low aromaticity^{35–38}. Our FT-ICR MS results show that formulae with this ‘microbial’ signature are strongly positively correlated with deforestation extent (Fig 3a) and negatively correlated with ^{14}C -DOC (Fig 3e). Overall, these patterns correspond well with our isotopic results, as well as with recent research on the controls of DOM composition that link landscape disturbance to the export of aged, aliphatic, protein-like, and microbial DOM^{18,30,38,39}. Consequently, we believe that the observed clear delineation of DOM composition concurrent with deforestation extent highlights the potential for future studies to fingerprint as well as develop unique molecular tracers for land-use change.

High Biolability of Aged DOC

To understand how deforestation controls the fate of DOM mobilized from disturbed soils, we conducted 28-day biolability incubations of stream water DOC inoculated with ambient microorganisms. We found the fraction of biolabile DOC (BDOC %) increased significantly with deforestation extent (Fig. S3a, Table S1) and was negatively correlated with ^{14}C -DOC (Fig. 2d, Table S1). Our linear model predicts that $19 \pm 3\%$ of DOC was biodegraded and respired to CO_2 in completely deforested catchments, compared to only $6.1 \pm 3.1\%$ in the pristine forested catchments.

Our data indicate that aged DOC mobilized from disturbed soils is substantially more biolabile than recently fixed C sourced from forested catchments. The compositional differences outlined in the section above explain this observed difference in biolability; DOM found in the deforested catchments with high H/C ratios (i.e. energy-rich), high abundance of N-containing formulae, and low aromaticity, is known to be highly biolabile^{40,41,42}. Indeed, our results show that the relative abundance of such formulae were positively correlated with BDOC (red points, Fig 3c). Conversely, molecular formulae assigned as polyphenolics and condensed aromatics are often stable over the timescale of water transit within these catchments⁴³. Formulae with these characteristics were negatively correlated with BDOC (blue points, Fig 3c).

The high biolability of aged DOC derived from deforested and agriculturally impacted soils observed in this study adds support to the emerging understanding that DOM biolability is independent of age. Recent glacier and permafrost studies have challenged the paradigm that old DOC is refractory by demonstrating high biolability of aged C^{20,43–45}. Taken together with the results here this suggests biolability is driven by the physico-chemical conditions

under which OM is formed and preserved and not just solely time since photosynthesis^{46–48}. In deeper soil horizons of the forested catchments in the Congo Basin, SOC has most likely been stabilized via organo-mineral complexation and/or physical disconnection from decomposers and enzymes. Subsequent deforestation and removal of surface soils then alters the physico-chemical conditions of these deeper layers, resulting in the breakdown of organo-mineral complexes and the loss of physical protection, ultimately leading to the release and mobilization of aged but chemically biolabile OM to aquatic ecosystems.

The observed high biolability of DOC in deforested catchments may lead to higher rates of respiration of OC relative to forest catchments. In both forested and deforested catchments, dissolved oxygen (DO) undersaturation indicates that respiration dominates over photosynthesis (Fig S4b, Table S1). In the deforested streams, however, the byproduct of respiration, dissolved CO₂, was ~900 ppm higher than in forested streams (Fig S4c, Table S1). Moreover, stream water temperatures were ~5° C higher (Fig. S4d, Table S1), potentially facilitating faster rates of bacterial respiration⁴⁹. Similar agricultural land-use driven warming of stream ecosystems has been observed in the Amazon Basin and was attributed to the loss of both riparian shade and forest transpiration⁵⁰. Collectively, these BDOC, DO, CO₂, and temperature results suggest that deforested catchments mineralize a greater proportion of DOC than forested catchments. Hence, streams draining deforested catchments are likely to outgas both more and older C as CO₂.

Impact of Land Use Change on Carbon Yields

Ultimately, the absolute impact of the loss of pristine tropical forests on the mobilization of DOM depends on the difference in size and quality of DOM fluxes between deforested and forested catchments. Across our 19 catchments, DOC concentration was negatively related to deforestation extent (Fig. S4d). To estimate water yields for the forested and deforested endmembers, we used a regionally calibrated precipitation model (See methods) that incorporates infiltration and plant evapotranspiration (ET). Owing to the higher rates of ET in the pristine forest catchments, our model predicts they export 0.41 m yr⁻¹ of water while deforested catchments export 0.59 m yr⁻¹ (Table 1).

Given these water yields and the DOC concentrations measured during the wet season (when >90% of annual discharge occurs, Fig. S5a), we estimate that pristine forests yield ~1,597 kg DOC km⁻² yr⁻¹, more than double the yield than that of deforested catchments (~708 kg km⁻² yr⁻¹, Table 1, Fig. S5b). We attribute this to the simple fact that in general, above- and below-ground productivity in central African forests is significantly higher than croplands, and therefore more OC is available to be mobilized into streams^{2,51}. Importantly, despite the significantly higher bulk DOC yields from forests, they do not export more BDOC than deforested catchments (Table 1, Fig. S5c). This is due to the higher BDOC concentrations observed in the deforested catchments. These estimated yields, together with the higher CO₂ concentrations and temperatures observed in deforested catchments, suggest that the loss of forests and conversion to agriculture increases both the rate of aquatic C respiration and the proportion of mineralized SOC available for outgassing from streams.

Using the above DOC yields, we tested whether the observed DOC isotopic and DOM compositional trends with deforestation could have resulted simply from loss of modern

forest vegetation that masked background inputs of old OC in the forest sites. An isotopic mass-balance model was used to derive the hypothetical ^{14}C value of modern DOC ($\text{DOC}_{\text{young}}$) needed to mask old DOC inputs and produce a composite forest signature ($\text{DOC}_{\text{forest}}$) of 19.0‰ (Fig. 2a). The model yielded a super-modern $\text{DOC}_{\text{young}}$ value of 177‰, which is significantly higher than recent leaf litter (~25-30‰), the most enriched SOC in Kahuzi-Biega (65.2‰, 2.5cm depth, Table S2), and sites from throughout the Congo Basin (50.4-93.7‰)⁵². This suggests that forests could not realistically mask the equivalent export of old DOC as from deforested catchments (supplemental methods). Moreover, DOM from deforested catchments exhibited unique molecular formulae relative to forested catchments (Fig. S6). These formulae were predominantly heteroatomic and nearly identical to the assemblage correlated with older DOC (blue points, Fig. 3e). Simply put, these formulae do not exist in the forested catchments and thus represent an additional and likely older source of DOC to deforested catchments.

Reversing the Forest Carbon Sink

Our results suggest that deforestation and the subsequent disturbance from agricultural land use reverses microbially-mediated C stabilization in deep (forest) soils and increases the downstream export of biolabile and aged OC derived from deeper soil horizons. Deforestation therefore interrupts these natural C-cycling pathways and hastens the mobilization, biomineralization, and transfer of old soil C to the atmosphere via the aquatic pathway.

Our coupled isotope results of catchment DOC and pristine forest SOC suggest that SOC originating from at least 0.5m is being mobilized to rivers in deforested catchments (Fig. 2c). This half-meter soil denudation depth may also be conservative, since the higher rates of biomineralization of aged OC from deeper soils may preferentially remove old C and result in a more enriched ^{14}C -DOC signature (shifting the apparent bulk signature towards a younger, shallower source). Regardless, this process signals a rapid loss of post-deforestation surface soils that have accumulated over hundreds to thousands of years of weathering.

The population of the DRC has grown from 15 million to 81 million people since the end of the Belgian colonial era in 1960 and is projected to grow more than 4-fold by 2100^{53,54}. To prevent an exacerbation of the patterns observed in this study and reduce erosion, maintain soil fertility, and retain previously stabilized C, the implementation of modified agricultural techniques based as soil conservation practices (e.g., terracing, buffer strips, incorporation of organic residues, etc.) will be required⁵⁵. Ultimately, we suggest that the retention of old and biolabile SOC that is currently stabilized and isolated from the modern C cycle is dependent on the conservation of forests and the related deceleration of land-use conversion in eastern Congo.

Methods

Site Description and Deforestation Extent Classification

The 19 catchments sampled for this study lie on the western side of Lake Kivu to the north and south of the city of Bukavu, Democratic Republic of Congo (Figure 1). We selected the region near Bukavu for this study due to the proximity of contrasting agricultural land-use and pristine forests. The pristine forest catchments, found almost exclusively within the protected Kahuzi-Biéga National Park boundaries, are dominated by a mixed, evergreen, broadleaf tree assemblage. Areas of deforested cropland are nearly treeless with a patchwork of small agricultural plots usually containing a mix of maize, beans, sorghum, banana, onion, cassava, and unplanted bare soil. Catchment boundaries were delineated using the TauDEM terrain analysis tool⁵⁶ along with a 1 arc second (c. 30m) digital elevation model (DEM)⁵⁷ and the GPS locations of our sampling points. Catchments were then uploaded to Google Earth Engine and analyzed for the fraction deforested using the MODIS 2013 Land Cover dataset (MCD12Q1)⁵⁸. Because historically forests covered the entire Kivu region prior to widespread human settlement²⁶, all non-forested land cover was considered “deforested” for the purpose of this study. As a result, deforested fractions were calculated as the fraction of the catchment containing no evergreen broadleaf forest or mixed forest, the only two forest classifications contained by the study catchments (MODIS classifications 2 and 5, respectively). Temporal changes in deforestation extent were assessed with historic ESA Climate Change Initiative (CCI) Land Cover data (<http://maps.elie.ucl.ac.be/CCI/viewer/index.php>) and found to be minimal over the past decade.

Sample Collection and Measurement

Water was collected from 19 streams near lake Kivu, Democratic Republic of Congo during the wet season in April of 2017. The wet season was chosen because it comprises more than 9 months of the year and represents nearly all of the annual water flux through streams (>90%). Streams were well mixed and varied in width from approximately 1 to 3 meters. All samples were collected from the thalweg of the streams at approximately 15cm depths below the water surface. Field measurements for dissolved oxygen (DO), pH, and temperature were taken with a pre-calibrated YSI ProDSS multimeter sonde. Dissolved carbon dioxide (CO₂) concentrations were measured with a pre-calibrated EOSense CO₂ Concentration probe (eosGP) that was allowed to equilibrate with the streamwater for at least 45 minutes. All water samples were filtered in the field with pre-combusted (450°C > 5 hours) 0.7 um glass microfiber filters into pre-washed and 1N HCl acid-leached polycarbonate bottles. Water samples were preserved via acidification to a pH of 2 with 12N HPLC-grade HCl the same day of sampling. The acidified water samples were analyzed for dissolved organic carbon (DOC) concentrations via high-temperature catalytic oxidation on a Shimadzu TOC-L CPH total organic carbon analyzer at Florida State University, Tallahassee, FL, US using established methodology⁵⁹. Soil samples were taken from three 22.5cm and one 75cm soil cores extracted from the pristine forest in Kahuzi-Biéga National Park (S2.31314, E28.75471). In addition, plant litter samples were taken from the forest floor around the soil cores. From each depth, approximately 100 grams of soil were collected and air-dried for 48 hours before being sealed and transported to the laboratory at ETH Zurich where soils were dried in a drying oven (50°C) and subsequently ball milled.

Carbon Isotope Analyses

For each site, 500ml of filtered and acidified water were sent to the National Ocean Sciences Accelerator Mass Spectrometry (NOSAMS, <http://www.whoi.edu/nosams/home>) laboratory in Woods Hole, MA for analysis of $\delta^{13}\text{C}$ -DOC and ^{14}C -DOC. Prepared soil and litter samples were analyzed at ETH Zurich for $\delta^{13}\text{C}$ -SOC using an elemental analyzer (Flash EA, Thermo Fisher Scientific, MA, US) coupled to a Delta^{plus}XP Isotope Ratio Mass Spectrometer via a 6-port valve and a ConFlo III interface (both Finnigan MAT, Bremen, Germany)^{60,61}. Soil sub-samples were sent to the Max Planck Institute for Biogeochemistry in Jena, Germany for ^{14}C -SOC analysis. Soil samples were combusted and graphitized following Steinhof et al. (2017)⁶² prior to analysis on a MICADAS ^{14}C AMS system (Ionplus AG, Dietikon, Switzerland). Leaf litter samples were assigned a modern radiocarbon value (+25‰) based on the 2016-2017 atmospheric CO_2 radiocarbon content⁶³.

FT-ICR MS Analysis

DOM in stream water samples was isolated for FT-ICR MS analysis via solid-phase extraction (SPE) with 100mg Bond Elut (Agilent Technologies) styrene-divinylbenzene copolymer (PPL) columns. Depending on a sample's DOC concentration, the volume used for extraction was adjusted such that 50 μg of C was eluted with 1ml of HPLC-grade methanol into a pre-combusted glass vial. The molecular composition of PPL-extracted DOM was determined using the 21-Tesla FT-ICR MS at the National High Magnetic Field Laboratory (NHMFL) at Florida State University, Tallahassee, FL, USA^{64,65}. Negative ions were generated by injecting the extracted sample into the mass spectrometer via negative electrospray ionization (negative ESI) at a flow rate of 500 nL min^{-1} . Mass spectra were generated as the sum of 100 individual spectra scans for each sample. See supporting text for formula assignment methods.

Biolability Incubation Experiments

Bioincubations of DOC (BDOC) were performed using established methods⁵⁹. Briefly, bioincubations were initiated by injecting 30mL of 0.7 μm filtered stream water into six pre-evacuated and pre-weighed 60mL borosilicate serum vials. Three serum vials were immediately acidified to a pH of 2 (t0) using 12N HPLC-grade HCl and the remaining three vials were allowed to incubate in the dark at room temperature for 28 days (t28) before acidification to a pH of 2. Each serum vial was then weighed, re-pressurized with helium, and allowed to equilibrate for one day before the concentration of CO_2 in the headspace was analyzed on a gas chromatograph at Florida State University, USA. Using Henry's law, CO_2 concentrations (equivalent to total dissolved inorganic carbon (DIC) concentrations at pH of 2) were determined by the volume of water in each serum vial and the concentration of CO_2 in the headspace. The difference in DIC concentrations between the averaged t28 and t0 timepoints was attributed to CO_2 produced by microbial respiration during the 28-day incubation. BDOC percentages were calculated by the ratio of C as CO_2 produced to the initial (t0) DOC concentration⁵⁹.

Water and DOC Yield Estimates

Area-weighted annual water yields were determined for the pristine forested and deforested endmembers using the US Army Corps of Engineers Hydrologic Engineering Center's Hydrologic Modeling System (HEC-HMS, <http://www.hec.usace.army.mil/software/hechms/>) paired with soil-infiltration, vegetation transpiration, and geomorphologic constraints for the Lake Kivu region. The model was calibrated with hourly-precipitation and runoff data sourced from the Goma Volcanic Observatory in Goma, DR Congo on the north side of Lake Kivu. Sampling point GPS-located Tropical Rainfall Measuring Mission (TRMM, <https://pmm.nasa.gov/TRMM>) precipitation data extrapolated over the total catchment area were used to estimate total annual precipitation ($\text{m}^3 \text{yr}^{-1}$) for each catchment. End-member-weighted water yields (proportion of precipitation as runoff, mm yr^{-1}) were then assigned to each catchment by deforestation extent. Total annual water yields for each catchment were then calculated by multiplying the modeled water yields by the total catchment area. Approximate annual DOC and BDOC yields were then calculated by multiplying the catchment-specific wet-season DOC and BDOC concentrations by the modeled annual water yields.

Statistical analyses

All least squares regression analyses, including the determination of 95% confidence intervals, were performed with Graphpad Prism 6.0 software. Standard errors of predicted values were calculated using the *Statsmodels* python package⁶⁶. FT-ICR MS data analysis for compound class statistics, heteroatomic content, and Spearman's rank correlations were performed with the *fouriertransform* Python package⁶⁷ (<https://github.com/FluvialSeds/fouriertransform>).

Supplementary Material

Refer to Web version on PubMed Central for supplementary material.

Acknowledgements

We would like to thank our network of collaborators at the International Institute of Tropical Agriculture and the Université Catholique de Bukavu in DR Congo for their local expertise and logistical assistance. Funding for this research was provided by the Winchester Fund at Florida State University. This work was partially supported by National Science Foundation grants OCE 1464396 to R.G.M.S., and DMR-1157490 and DMR-1644779 to the National High Magnetic Field Laboratory. K.V.O. received funding from FNRS. A.M.H. and S.E.T. received funding from the European Research Council (ERC) under the European Union's Horizon 2020 research and innovation programme (grant agreement No. 695101 (14Constraint)).

References

1. Köchy M, Hiederer R, Freibauer A. Global distribution of soil organic carbon--Part 1: Masses and frequency distributions of SOC stocks for the tropics, permafrost regions, wetlands, and the world. *Soil*. 2015; 1:351–365.
2. Don A, Schumacher J, Freibauer A. Impact of tropical land-use change on soil organic carbon stocks--a meta-analysis. *Glob Chang Biol*. 2011; 17:1658–1670.
3. Schlesinger WH, Andrews JA. Soil respiration and the global carbon cycle. *Biogeochemistry*. 2000; 48:7–20.

4. Houghton RA. The annual net flux of carbon to the atmosphere from changes in land use 1850–1990. *Tellus B Chem Phys Meteorol.* 1999; 51:298–313.
5. Guo LB, Gifford RM. Soil carbon stocks and land use change: a meta analysis. *Glob Chang Biol.* 2002; 8:345–360.
6. Stanley EH, Powers SM, Lottig NR, Buffam I, Crawford JT. Contemporary changes in dissolved organic carbon (DOC) in human-dominated rivers: is there a role for DOC management? *Freshw Biol.* 2012; 57:26–42.
7. Schelker J, Grabs T, Bishop K, Laudon H. Drivers of increased organic carbon concentrations in stream water following forest disturbance: Separating effects of changes in flow pathways and soil warming. *Journal of Geophysical Research: Biogeosciences.* 2013; 118:1814–1827.
8. Chow AT, Dahlgren RA, Harrison JA. Watershed sources of disinfection byproduct precursors in the Sacramento and San Joaquin Rivers California. *Environ Sci Technol.* 2007; 41:7645–7652. [PubMed: 18075069]
9. Chen X, Driscoll CT. Watershed land use controls on chemical inputs to lake ontario embayments. *J Environ Qual.* 2009; 38:2084–2095. [PubMed: 19704151]
10. Meyer JL, Tate CM. The Effects of Watershed Disturbance on Dissolved Organic Carbon Dynamics of a Stream. *Ecology.* 1983; 64:33–44.
11. Cronan CS, Piampiano JT. Influence of land use and hydrology on exports of carbon and nitrogen in a Maine river basin. *Journal of.* 1999
12. Moore S, et al. Deep instability of deforested tropical peatlands revealed by fluvial organic carbon fluxes. *Nature.* 2013; 493:660–663. [PubMed: 23364745]
13. Rixen T, Baum A, Wit F, Samiaji J. Carbon Leaching from Tropical Peat Soils and Consequences for Carbon Balances. *Front Earth Sci.* 2016; 4:563.
14. Butman DE, Wilson HF, Barnes RT, Xenopoulos MA, Raymond PA. Increased mobilization of aged carbon to rivers by human disturbance. *Nat Geosci.* 2014; 8:112–116.
15. Lu YH, et al. Effects of land use on sources and ages of inorganic and organic carbon in temperate headwater streams. *Biogeochemistry.* 2014; 119:275–292.
16. Raymond PA, Bauer JE. Riverine export of aged terrestrial organic matter to the North Atlantic Ocean. *Nature.* 2001; 409:497–500. [PubMed: 11206542]
17. Mayorga E, et al. Young organic matter as a source of carbon dioxide outgassing from Amazonian rivers. *Nature.* 2005; 436:538–541. [PubMed: 16049484]
18. Barnes RT, Butman DE, Wilson HF, Raymond PA. Riverine Export of Aged Carbon Driven by Flow Path Depth and Residence Time. *Environ Sci Technol.* 2018; doi: 10.1021/acs.est.7b04717
19. Mann PJ, et al. Utilization of ancient permafrost carbon in headwaters of Arctic fluvial networks. *Nat Commun.* 2015; 6
20. Hood E, et al. Glaciers as a source of ancient and labile organic matter to the marine environment. *Nature.* 2009; 462:1044–1047. [PubMed: 20033045]
21. Nachtergaele, F, , et al. Harmonized world soil database. Wageningen: ISRIC; 2009.
22. Dargie GC, et al. Age, extent and carbon storage of the central Congo Basin peatland complex. *Nature.* 2017; 542:86–90. [PubMed: 28077869]
23. Ickowitz, A, Slayback, D, Asanzi, P, Nasi, R. Agriculture and deforestation in the Democratic Republic of the Congo: A synthesis of the current state of knowledge. CIFOR; 2015.
24. Hansen MC, et al. High-resolution global maps of 21st-century forest cover change. *Science.* 2013; 342:850–853. [PubMed: 24233722]
25. Potapov PV, et al. Quantifying forest cover loss in Democratic Republic of the Congo, 2000–2010, with Landsat ETM+ data. *Remote Sens Environ.* 2012; 122:106–116.
26. Kabonyi C, Roche E, Gerrienne P. Paléoenvironnements et paléoclimats durant le Pléistocène supérieur et l’Holocène sur la dorsale occidentale du Kivu en République Démocratique du Congo. *European Scientific Journal.* 2015; 11:38–63.
27. Bostrom B, Comstedt D, Ekblad A. Isotope fractionation and ¹³C enrichment in soil profiles during the decomposition of soil organic matter. *Oecologia.* 2007; 153:89–98. [PubMed: 17401582]

28. Rumpel C, Kögel-Knabner I. Deep soil organic matter—a key but poorly understood component of terrestrial C cycle. *Plant Soil*. 2011; 338:143–158.
29. Koch BP, Dittmar T. From mass to structure: an aromaticity index for high-resolution mass data of natural organic matter. *Rapid Commun Mass Spectrom*. 2006; 20:926–932.
30. Wagner S, et al. Linking the Molecular Signature of Heteroatomic Dissolved Organic Matter to Watershed Characteristics in World Rivers. *Environ Sci Technol*. 2015; 49:13798–13806. [PubMed: 26153846]
31. Riedel T, et al. Molecular Signatures of Biogeochemical Transformations in Dissolved Organic Matter from Ten World Rivers. *Front Earth Sci*. 2016; 4:G01004.
32. D'Andrilli J, Cooper WT, Foreman CM, Marshall AG. An ultrahigh-resolution mass spectrometry index to estimate natural organic matter lability. *Rapid Commun Mass Spectrom*. 2015; 29:2385–2401. [PubMed: 26563709]
33. Stubbins A, et al. Illuminated darkness: molecular signatures of Congo River dissolved organic matter and its photochemical alteration as revealed by ultrahigh precision mass spectrometry. *Limnol Oceanogr*. 2010; 55:1467–1477.
34. Spencer RGM, et al. Utilizing chromophoric dissolved organic matter measurements to derive export and reactivity of dissolved organic carbon exported to the Arctic Ocean: A case study of the Yukon River, Alaska. *Geophys Res Lett*. 2009; 36
35. Kellerman AM, et al. Unifying Concepts Linking Dissolved Organic Matter Composition to Persistence in Aquatic Ecosystems. *Environ Sci Technol*. 2018; 52:2538–2548. [PubMed: 29393627]
36. Kaiser K, Kalbitz K. Cycling downwards--dissolved organic matter in soils. *Soil Biol Biochem*. 2012; 52:29–32.
37. Kögel-Knabner I, Totsche KU, Raber B. Desorption of Polycyclic Aromatic Hydrocarbons from Soil in the Presence of Dissolved Organic Matter: Effect of Solution Composition and Aging. *J Environ Qual*. 2000; 29:906–916.
38. Wilson HF, Xenopoulos MA. Effects of agricultural land use on the composition of fluvial dissolved organic matter. *Nat Geosci*. 2008; 2:37.
39. Creed IF, et al. Global change-driven effects on dissolved organic matter composition: Implications for food webs of northern lakes. *Glob Chang Biol*. 2018
40. Berggren M, Laudon H, Haei M, Ström L, Jansson M. Efficient aquatic bacterial metabolism of dissolved low-molecular-weight compounds from terrestrial sources. *ISME J*. 2010; 4:408–416. [PubMed: 19907505]
41. van Hees PAW, Jones DL, Finlay R, Godbold DL, Lundström US. The carbon we do not see—the impact of low molecular weight compounds on carbon dynamics and respiration in forest soils: a review. *Soil Biol Biochem*. 2005; 37:1–13.
42. Kalbitz K, et al. Changes in properties of soil-derived dissolved organic matter induced by biodegradation. *Soil Biol Biochem*. 2003; 35:1129–1142.
43. Spencer RGM, et al. Detecting the signature of permafrost thaw in Arctic rivers. *Geophys Res Lett*. 2015; 42
44. Singer GA, et al. Biogeochemically diverse organic matter in Alpine glaciers and its downstream fate. *Nat Geosci*. 2012; 5:710–714.
45. Spencer RGM, et al. Source and biolability of ancient dissolved organic matter in glacier and lake ecosystems on the Tibetan Plateau. *Geochim Cosmochim Acta*. 2014; 142:64–74.
46. Schmidt MWI, et al. Persistence of soil organic matter as an ecosystem property. *Nature*. 2011; 478:49–56. [PubMed: 21979045]
47. Kögel-Knabner I. The macromolecular organic composition of plant and microbial residues as inputs to soil organic matter. *Soil Biol Biochem*. 2002; 34:139–162.
48. Deneff, K, Planet, AF, Six, J. Characterization of soil organic matter. *Soil Carbon Dynamics: An Integrated Methodology*. Kutsch, WL, Bahn, M, Heinemeyer, A, editors. Cambridge University Press; 2009. 91–126.
49. Demars BOL, et al. Temperature and the metabolic balance of streams. *Freshw Biol*. 2011; 56:1106–1121.

50. Macedo MN, et al. Land-use-driven stream warming in southeastern Amazonia. *Philos Trans R Soc Lond B Biol Sci.* 2013; 368
51. Baccini A, Laporte N, Goetz SJ, Sun M. A first map of tropical Africa's above-ground biomass derived from satellite imagery. *Environmentalist.* 2008
52. Spencer RGM, et al. An initial investigation into the organic matter biogeochemistry of the Congo River. *Geochim Cosmochim Acta.* 2012; 84:614–627.
53. Gerland P, et al. World population stabilization unlikely this century. *Science.* 2014; 346:234–237. [PubMed: 25301627]
54. United Nations. World Population Prospects 2017. 2017. Available at: <https://esa.un.org/unpd/wpp/>
55. Govers, G, Merckx, R, Van Oost, K, van Wesemael, B. Managing soil organic carbon for global benefits: a STAP technical report. Global Environmental Facility; Washington, DC: 2013.
56. Tarboton, D. [Accessed: February 2018] TauDEM Version 5. Hydrologic terrain analysis with parallel processing. <http://hydrology.usu.edu/taudem/taudem5/>
57. Nasa JPL. NASA Shuttle Radar Topography Mission Global 1 arc second. NASA LP DAAC. 2013; 15
58. Friedl MA, et al. MODIS Collection 5 global land cover: Algorithm refinements and characterization of new datasets. *Remote Sens Environ.* 2010; 114:168–182.
59. Drake TW, et al. The Ephemeral Signature of Permafrost Carbon in an Arctic Fluvial Network. *J Geophys Res Biogeosci.* 2018; doi: 10.1029/2017JG004311
60. Werner RA, Bruch BA, Brand WA. ConFlo III-an interface for high precision d13C and d15N analysis with an extended dynamic range. *Rapid Commun Mass Spectrom.* 1999; 13:1237–1241. [PubMed: 10407304]
61. Brooks PD, Geilmann H, Werner RA, Brand WA. Improved precision of coupled $\delta^{13}\text{C}$ and $\delta^{15}\text{N}$ measurements from single samples using an elemental analyzer/isotope ratio mass spectrometer combination with a post-column six-port valve and selective CO_2 trapping; improved halide robustness of the combustion reactor using CeO_2 . *Rapid Commun Mass Spectrom.* 2003; 17:1924–1926. [PubMed: 12876695]
62. Steinhof A, Altenburg M, Machts H. Sample Preparation at the Jena ^{14}C Laboratory. *Radiocarbon.* 2017; 59:815–830.
63. Turnbull JC, et al. Sixty years of radiocarbon dioxide measurements at Wellington, New Zealand: 1954–2014. *Atmos Chem Phys.* 2017; 17:14771–14784.
64. Smith DF, Podgorski DC, Rodgers RP, Blakney GT, Hendrickson CL. 21 Tesla FT-ICR Mass Spectrometer for Ultrahigh-Resolution Analysis of Complex Organic Mixtures. *Anal Chem.* 2018; 90:2041–2047. [PubMed: 29303558]
65. Hendrickson CL, et al. 21 Tesla Fourier Transform Ion Cyclotron Resonance Mass Spectrometer: A National Resource for Ultrahigh Resolution Mass Analysis. *J Am Soc Mass Spectrom.* 2015; 26:1626–1632. [PubMed: 26091892]
66. Seabold, S; Perktold, J. Statsmodels: Econometric and statistical modeling with python. Proceedings of the 9th Python in Science Conference; SciPy society Austin; 2010. 61
67. Hemingway JD. Fouriertransform: Open-Source Tools for FT-ICR MS Data Analysis. 2017

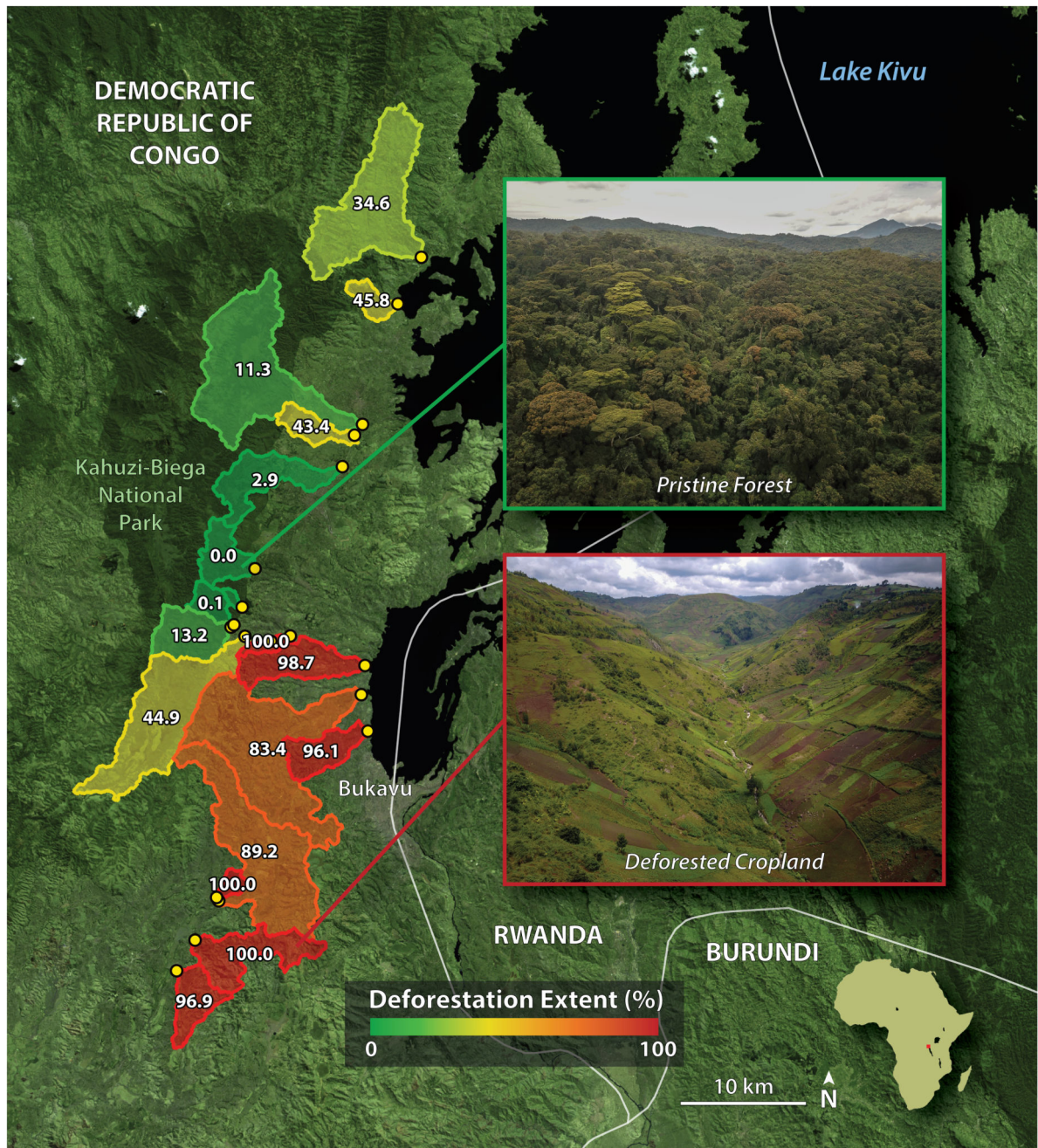


Figure 1. Sampling locations (yellow points) and catchment delineations for this study (n=19). Study catchments are colored from green to red according to their deforestation extent. White numbers overlaying each catchment indicate the areal percent of deforestation. Inlaid pictures show an aerial view of pristine forest (top) and deforested cropland (bottom). Basemap imagery sourced from Copernicus Sentinel-2 satellite data [2017].

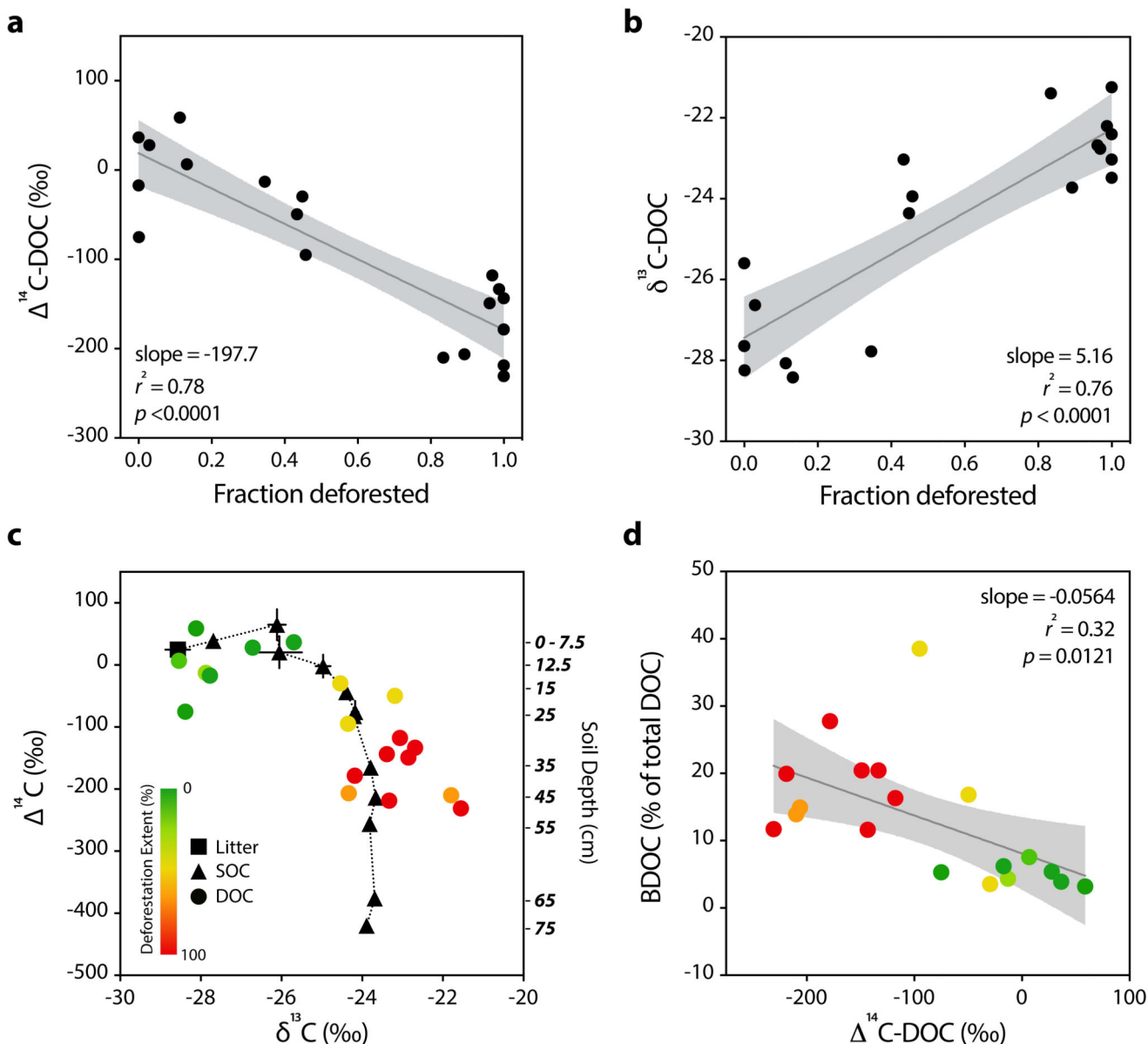


Figure 2. Isotopic indicators of stream DOC age, sources, and biolability.

a, least-squares regressions between the fraction of deforestation and $^{14}\text{C-DOC}$ ($y = -197.7x + 19.0$) and **b**, fraction of deforestation and $\delta^{13}\text{C-DOC}$ ($y = 5.16x - 27.4$) for all 19 catchments. **c**, ^{14}C versus $\delta^{13}\text{C}$ for streamwater DOC from 19 catchments (colored circles) and SOC at different soil depths (given on the right y-axis) from a core taken in the pristine forest (black triangles with dotted line). Litter (black square) represents leaves and detritus from the forest floor above the core. Green-to-red color bar indicates the fraction of deforestation of each catchment represented by the DOC point. Black error bars of the SOC data represent the standard deviation of values from the same depth of multiple cores, when available. **d**, least-squares regression between $^{14}\text{C-DOC}$ and biolabile DOC (BDOC) for all 19 catchments ($y = -0.056x + 8.12$). The deforestation extent of each point is represented by the color bar in

panel **c**. Gray bands indicate 95% confidence intervals for panels **a**, **b**, and **d**. ‘Modern’ radiocarbon value is +25‰ for panels **a**, **c**, and **d**.

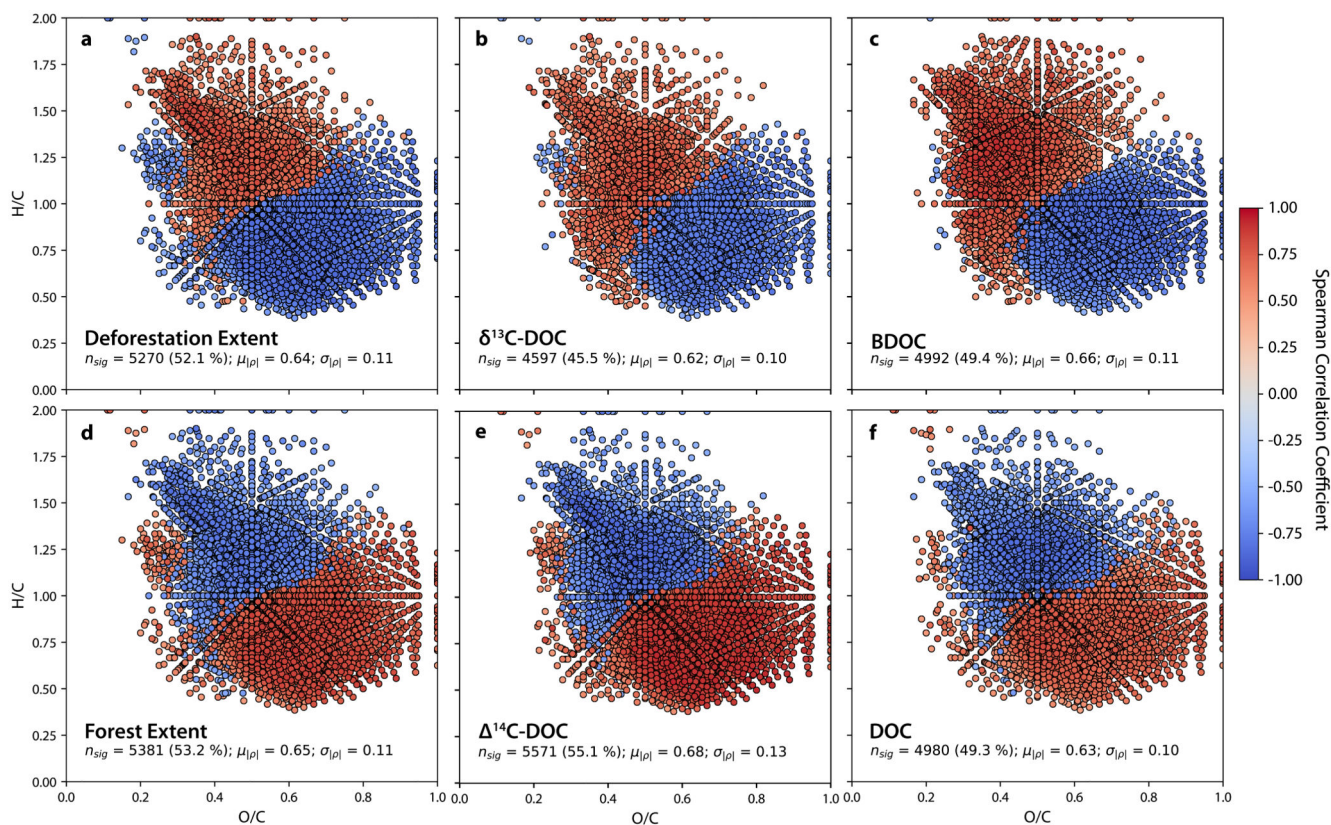


Figure 3. Van Krevelen diagrams of molecular formulae as a function of six environmental variables.

Spearman-rank correlations of relative intensities for each molecular formulae and **a**, deforestation extent; **b**, $\delta^{13}\text{C-DOC}$; **c**, BDOC; **d**, forest extent; **e**, $\Delta^{14}\text{C-DOC}$; and **f**, DOC concentration. Colors represent the correlation coefficient (ρ_s) between the relative intensity of each molecular formula and the given environmental variable. Red formulae (positive ρ_s) are more abundant in samples where the given environmental variable is high while blue formulae (negative ρ_s) are more abundant when the variable is low. The n_{sig} is the number of significantly correlated formulae for each variable. Proportion of common formulae comprised by n_{sig} are shown in parentheses. Also listed are the mean (μ) and standard deviation (σ) of the absolute value of $|\rho_s|$ for all formulae displayed in each panel.

Table 1
Predicted area-weighted annual fluxes of water, dissolved organic carbon, and biolabile dissolved organic carbon from pristine forest and deforested end-member catchments.

Error ranges are the standard error of the predicted end-member values from the linear regression. The Change (%) is the relative difference of the deforested fluxes compared to the pristine. Note that the percent change for BDOC is not statistically significant (n.s.).

	Water (m yr ⁻¹)	DOC (kg km ⁻² yr ⁻¹)	BDOC (kg km ⁻² yr ⁻¹)
Pristine Forest	0.41	1597 ± 262	78 ± 26
Deforested	0.59	674 ± 228	126 ± 22
Change (%)	+44%	-56%	+66% (n.s.)